

An experimental and computational investigation of structure and magnetism in pyrite $\text{Co}_{1-x}\text{Fe}_x\text{S}_2$: Chemical bonding and half-metallicity

K. Ramesha* and Ram Seshadri†
Materials Department and Materials Research Laboratory
University of California, Santa Barbara, CA 93106 USA

Claude Ederer‡
Materials Research Laboratory
University of California, Santa Barbara, CA 93106 USA

Tao He§ and M. A. Subramanian¶
DuPont Central Research and Development
Experimental Station, E328/219 Wilmington, DE 19880-0328

Bulk samples of the pyrite chalcogenide solid solutions $\text{Co}_{1-x}\text{Fe}_x\text{S}_2$ ($0 \leq x \leq 0.5$), have been prepared and their crystal structures and magnetic properties studied by X-ray diffraction and SQUID magnetization measurements. Across the solution series, the distance between sulfur atoms in the persulfide (S_2^{2-}) unit remains nearly constant. First principles electronic structure calculations using experimental crystal structures as inputs point to the importance of this constant S-S distance, in helping antibonding S-S levels pin the Fermi energy. In contrast hypothetical rock-salt CoS is not a good half metal, despite being nearly isostructural and isoelectronic. We use our understanding of the $\text{Co}_{1-x}\text{Fe}_x\text{S}_2$ system to make some prescriptions for new ferromagnetic half-metals.

PACS numbers: 71.20.-b, 72.25.-b, 75.47.-m, 85.75.-d

I. INTRODUCTION

The rapid development of spin valve-based magnetic read heads and the emergence of spintronics¹ has thrown up a need for new magnetic half-metals for spin injection, as well as the need for a better understanding of the underlying materials issues in magnetic half-metals.^{2,3} The recognition that pyrite CoS_2 is a ferromagnetic half-metal,^{4,5} and that half-metallicity is robust across the solid solution $\text{Co}_{1-x}\text{Fe}_x\text{S}_2$ ⁶ has led to considerable renewed efforts to understand this material.⁷ However, there is as yet no report on why the solid solution $\text{Co}_{1-x}\text{Fe}_x\text{S}_2$ is special: What are the unusual features in the crystal and electronic structure of the pyrites that result in its properties ?

Benoit and Néel first showed that cobalt pyrite CoS_2 is a ferromagnet.¹⁰ No other MX_2 compound ($X = \text{chalcogenide}$), or even MXY ($Y = \text{pnictide}$) is ferromagnetic.^{8,9} Jarrett *et al.*⁴ made magnetic and transport measurements on $\text{Co}_{1-x}\text{Fe}_x\text{S}_2$ which indicated itinerant electron ferromagnetism. FeS_2 ($x = 1$) is a d band semiconductor with filled octahedral t_{2g}^6 levels of Fe^{2+} level separated from empty e_g levels. As electrons are added ($0 \leq x \leq 1$) the compounds become conducting and ferromagnetic, even for x values as large as 0.97 (or electron concentrations as small as 0.03 in the e_g band). Over a wide range of x , the magnetic moment (in Bohr magnetons) obtained from saturation magnetization is precisely equal to the number of e_g electrons. DiTusa *et al.*¹¹ have recently argued that the dilute (x approaching 1) regions of the solid solution are worthy of closer examination and that near $x = 0.99$, an insulator-metal transition is al-

ready observed. They report a quantum critical point in the ferromagnetic-paramagnetic transition between $x = 0.972$ and $x = 0.964$.

Spin-polarized electronic structure calculations by Zhao, Callaway and Hayashibara⁵ found that CoS_2 is ferromagnetic, and nearly a half-metal, resembling the prototypic magnetic half-metal NiMnSb .¹² Yamada *et al.*¹³ have optimized the structure and Kwon *et al.*¹⁴ have performed LSDA+ U (LSDA = local spin density approximation) calculations on CoS_2 . Shishidou *et al.*¹⁵ have performed first principles calculations on CoS_2 with gradient corrections (GGA = generalized gradient approximation).

In a seminal paper, Mazin⁶ has shown from first-principles calculations that ferromagnetic half-metallicity is “robust” in the system $\text{Co}_{1-x}\text{Fe}_x\text{S}_2$, in the sense that in the region $0.85 \leq x \leq 0.25$ the compounds are perfect half metals, with moments precisely equal to the spin only values [$M(\mu_B)/\text{Co} = 1$] in agreement with the experiments of Jarrett *et al.*⁴ However, from point-contact Andreev reflection measurements, Cheng, Mazin and coworkers *et al.*¹⁶ determine the maximum *transport* half-metallicity to not exceed 61%. The maximum occurs near $x = 0.5$. The reduced half-metallicity is ascribed to sulfur deficiency in the samples, which interestingly, does not seem to affect magnetism.

In this contribution, we focus on the cobalt rich side of the pyrite $\text{Co}_{1-x}\text{Fe}_x\text{S}_2$ phase diagram. We obtain a detailed structural description of the compounds $0 \leq x \leq 0.5$ from Rietveld¹⁷ refinement of powder X-ray diffraction patterns. We also confirm from magnetic measurements that the samples behave in the manner described by Jarrett *et al.*⁴ We use the crystal structures as in-

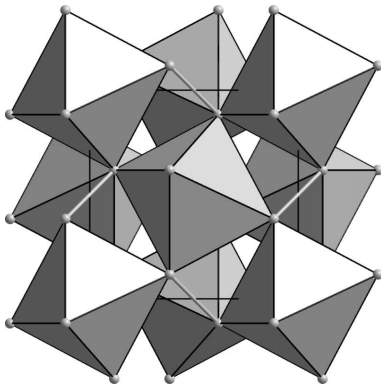


FIG. 1: MX_2 pyrite crystal structure showing MX_6 octahedra corner connected through X atoms which, in addition, are bonded (shown by sticks) to X atoms on neighboring octahedra. The coordination of X is $3(\text{M}) + 1(\text{X})$. X_2 sticks and M atoms (at the centers of the octahedra) form two interpenetrating fcc lattices and a structure related to NaCl.

puts for first principles electronic structure calculations based on the linear muffin-tin orbital method,²¹ both for pristine CoS_2 as well as the supercells $\text{Co}_{0.75}\text{Fe}_{0.25}\text{S}_2$ and $\text{Co}_{0.5}\text{Fe}_{0.5}\text{S}_2$. We use the crystal orbital hamiltonian population (COHP)¹⁹ to examine details of spin-polarized chemical bonding across the solid solution series, and examine the relation between chemical bonding and half-metallicity. A comparison with rock-salt CoS (whose spin polarized crystal and electronic structure have been calculated from first-principles) confirms the special features of the electronic structure of the pyrites.

II. EXPERIMENTAL

Samples of $\text{Co}_{1-x}\text{Fe}_x\text{S}_2$ ($0 \leq x \leq 0.5$) were prepared starting from the elements taken according to stoichiometry, by heating well-ground powders in evacuated, sealed silica ampoules for 1 week at 673 K. The powders were then reground, pelletized, resealed in evacuated silica ampoules, and heated for 873 K for 4 d. A final heating was performed at 973 K for one week, of samples that had been ground up and pelletized again. Powder X-ray diffraction patterns were collected on powders using overnight runs on a Scintag X2 diffractometer operating in the Bragg-Brentano θ - 2θ geometry. Data were recorded using $\text{CuK}\alpha$ radiation and a step size of 0.02° in 2θ . The data were subject to Rietveld refinement¹⁷ using the pyrite (space group $P\bar{a}3$, No. 205) structural model with the transition metal (Co or Fe) at $(0, 0, 0)$ and S at (x_S, x_S, x_S) with $x_S \approx 0.39$. The XND²⁰ Rietveld program was employed for the refinements.

Magnetic measurements were performed using a Quantum Design MPMS 5XL Magnetometer. Sample holders (gelatin capsules inserted in plastic drinking straws) held small solid pellets of the $\text{Co}_{1-x}\text{Fe}_x\text{S}_2$ phases. We have not corrected the measured magnetizations for any core

or sample-holder diamagnetism. Demagnetization corrections have not been performed.

III. COMPUTATIONAL METHODS

Linear muffin-tin orbital (LMTO) calculations²¹ within the atomic sphere approximation (ASA) were performed using the STUTTGART TB-LMTO-ASA program.¹⁸ Experimental crystal structures used as inputs for the calculations were obtained from X-ray Rietveld refinements from this study, unless otherwise mentioned. Typically, more than 300 irreducible k points within the primitive wedge of Brillouin zone were employed in the calculations. The generalized gradient approximation (GGA) for calculation of exchange correlation was employed following the Perdew-Wang prescription.²² This results in slightly larger moments over the von Barth-Hedin²³ LSDA, although not to the extent that CoS_2 is a perfect half metal as determined by Shishidou *et al.*¹⁵ Calculations including the effect of the spin-orbit interaction were also performed using a modified version of the LMTO code.²⁴ The implementation of the spin-orbit coupling into the otherwise scalar-relativistic LMTO formalism is analogous to the implementation described in²⁵ for the APW method. It was found that neither the states near the Fermi energy, not the magnetic moment were in any way affected by the inclusion of spin-orbit coupling. For ferromagnetic, rock-salt CoS, the cell volume (which is the sole free structural parameter) was optimized using full-potential linearized augmented plane wave (LAPW) calculations using the WIEN2K code.²⁶ Exchange correlation was considered following the Perdew-Burke-Ernzerhof²⁷ parametrization.

IV. RESULTS

A. Crystal structure

Powder X-ray diffraction revealed all compounds in the series to be single phase, and well-fitted by Rietveld profile refinement to the pyrite crystal structure described in FIG. 1. Results of the X-ray refinement are summarized in FIG. 2(a), which shows data for the two extreme compositions [$x = 0.0$ and $x = 0.5$] in the series studied here. The cubic a cell parameter varies linearly with x , as shown in FIG. 2(b) indicating the formation of a homogeneous solid-solution. Careful analysis does however suggest a broadening in peak profiles as x increases in $\text{Co}_{1-x}\text{Fe}_x\text{S}_2$. The decrease in the a lattice parameter as a function of increasing x (substitution of Co by Fe) arises from the different sizes of these ions; six-coordinate, low spin Co^{2+} has an ionic radius of 0.65 \AA whereas the corresponding radius for Fe^{2+} is 0.61 \AA .²⁸ The single internal parameter in the pyrite crystal structure is the position (x_S, x_S, x_S) of S. We have used refined values of

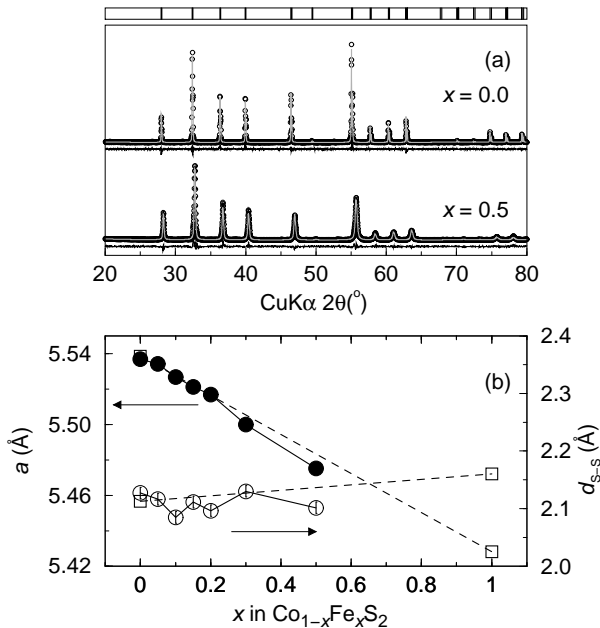


FIG. 2: (a) Powder X-ray Rietveld refinement of CoS_2 ($x = 0$) and $\text{Co}_{0.5}\text{Fe}_{0.5}\text{S}_2$ ($x = 0.5$). Data (circles), the Rietveld fit and the difference profiles are shown for each compound. Vertical lines at the top of the plot indicate expected peak positions. (b) Filled circles: Evolution of the a cell parameter (in Å) with x of the solid solution $\text{Co}_{1-x}\text{Fe}_x\text{S}_2$. Error bars are smaller than the circles. The dashed lines connects published crystal structure^{29,30} data on the end members (squares). Open circles: S-S distances as function of x . The dashed line connects published²⁹ data (squares).

x_S and a to calculate S-S distances across the solid solution series. Within experimental error, we find nearly no change in the S-S distance as a function of x as seen in FIG. 2(b). This is an important experimental observation, which we discuss at length at a later stage. In FIG. 2(b) we also show for comparison, structural data for the end-members CoS_2 ²⁹ and FeS_2 .³⁰

B. Magnetism

Zero field cooled (ZFC) and field-cooled (FC) magnetization M as a function of temperature recorded on $\text{Co}_{1-x}\text{Fe}_x\text{S}_2$ are indicated in FIG. 3(a). ZFC data were recorded in a field of 1000 Oe upon warming from 5 K after cooling from room temperature under zero field. FC data were also collected upon warming from 5 K, after the samples were cooled under a 1000 Oe field. All samples show evidence for ferromagnetism, with T_c s below 155 K. There is almost no ZFC/FC separation in any of the samples, suggesting the samples are homogeneous, and also that they combine high permeability with low saturation fields. Clear ferromagnetic T_c onsets as well as widths of the transition are best seen from plots of MT vs. T displayed in FIG. 3(b). The T_c onset does

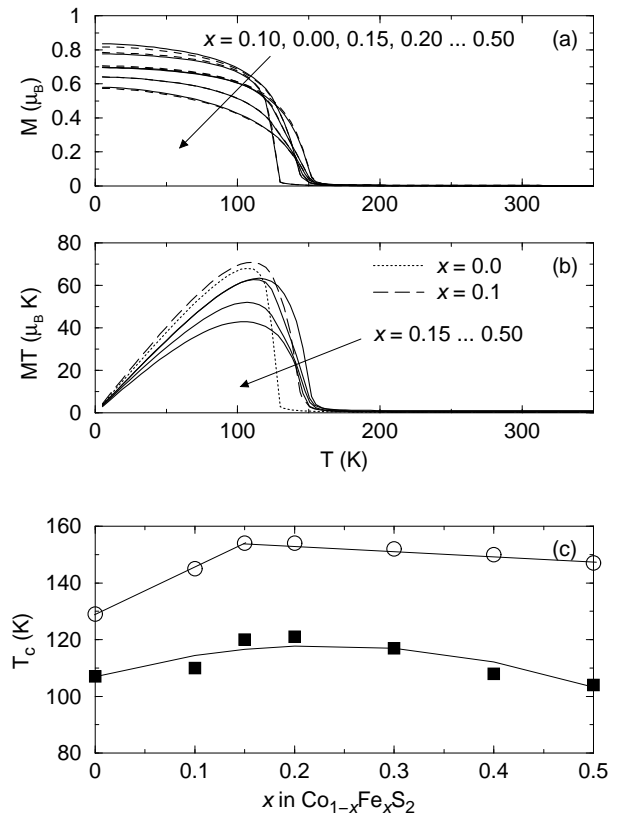


FIG. 3: (a) Zero-field cooled (dashed lines) and field-cooled magnetization as a function of temperature of the $\text{Co}_{1-x}\text{Fe}_x\text{S}_2$ samples. (b) Field-cooled MT vs. T . (c) T_c onset (circles) and midpoint, corresponding to the maximum value (squares) obtained from the MT vs. T plot, as a function of x . The lines are guides to the eye.

not seem to depend very much on x , and after an initially increasing with x , almost remains constant as seen in FIG. 3(c). Data were acquired under relatively high field (1000 Oe) so even small clusters of spins are sufficient for the magnetization to rise. The midpoints of the MT vs. T traces are therefore better indication of ferromagnetic T_c . These are also shown in FIG. 3(c), and are seen to initially increase with x and then decrease. The constant width of the transition [difference between T_c (onset) and T_c (midpoint)] for the different values of x reflects that all the samples are homogeneous, and the transition is not due to small ferromagnetic clusters.

Magnetization at 5 K is displayed in FIG. 4(a). None of the samples showed any significant hysteresis implying $\text{Co}_{1-x}\text{Fe}_x\text{S}_2$ is a soft ferromagnet. Therefore only the positive M vs. H quadrant is displayed. All the samples display saturation at fields well below 1 T. The saturation magnetization in Bohr magnetons (μ_B) is plotted as a function of x in FIG. 4(b). The dashed line is the expected spin-only value assuming each e_g electron contributes $1 \mu_B$ per formula unit to the magnetization. Only the parent CoS_2 phase is seen to have a satura-

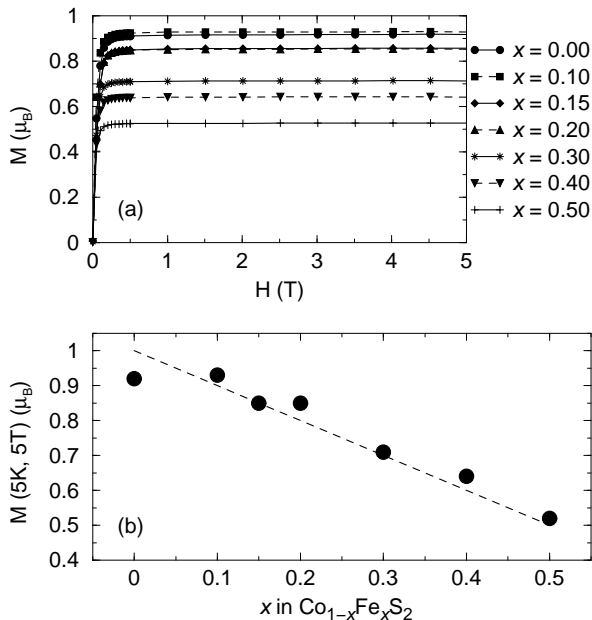


FIG. 4: (a) Magnetization at 5 K as a function of field. Since none of the samples show appreciable hysteresis, only the positive quadrant is displayed. Data were acquired from 5 T through 0 T. The dashed line is the expected spin only value assuming every e_g electron contributes $1 \mu_B$. (b) Saturation magnetization (5 K, 5 T) as a function of x .

tion magnetization less than the spin-only value. Starting from $x = 0.1$ through $x = 0.5$, all samples display spin-only behavior. This is an indication that all the samples except $x = 0.0$ are within experimental error, perfect half-metals in terms of their being no “leak” in the magnetization from majority to minority spin states. Such leaking is prevented by the complete absence of there are no minority spin states at the Fermi energy. Our results, for both ferromagnetic T_c (midpoint) as well as saturation magnetization are nearly identical with those obtained by Jarrett *et al.*⁴

C. Electronic structure

An number of authors have provided detailed electronic structure descriptions of CoS_2 .^{5,13,14,15} Mazin⁶ has examined magnetism across the series $\text{Co}_{1-x}\text{Fe}_x\text{S}_2$. The purpose of this section is to use structure refinements as inputs to obtain first principles electronic structures, and in particular, to calculate COHPs so that trends in spin-polarized bonding across the solid solution series can be obtained.

Figure 5 shows total LMTO densities of state (DOS) in the two spin states for (a) *hcp* Co metal, for (b) CoS_2 (using the $Pa\bar{3}$ crystal structure obtained from X-ray refinements performed here) and (c) FeS_2 using the crystal structure reported by Finklea *et al.*³⁰; SG. $Pa\bar{3}$, $a =$

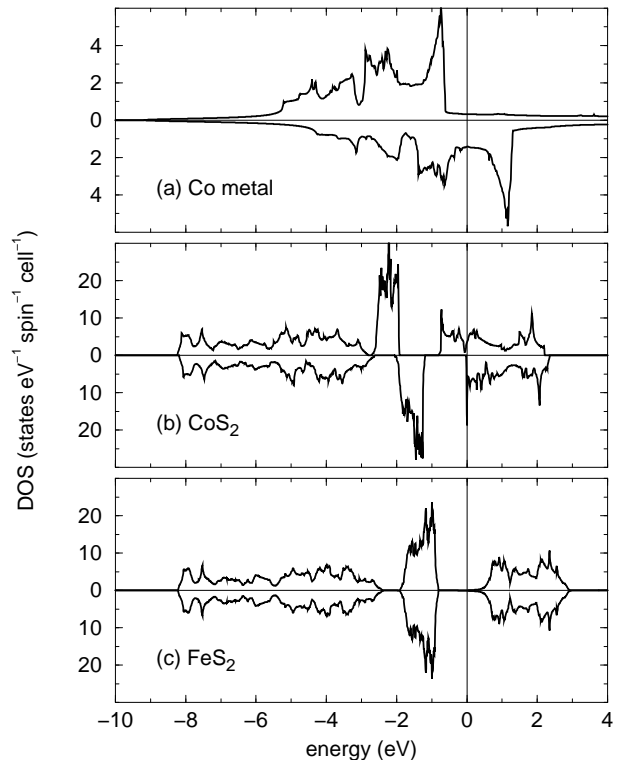


FIG. 5: (a) LMTO densities of state of *hcp* Co metal. (b) Densities of state of CoS_2 . The origin on the energy axis in (a) and (b), indicated by a vertical line, are the respective Fermi energies. (c) Densities of state of non-magnetic FeS_2 split into two spin directions. The energy axis has been shifted in (c) as described in the text. The upper and lower parts of each panel indicate respectively, majority and minority spin states.

5.4281 \AA , $x_S = 0.38504$. Fermi energies are taken as 0 on the energy axis in panels (a) and (b). On going from Co metal to CoS_2 , we observe a narrowing of d states as well as the effects of the octahedral crystal generated by the S_2^{2-} moieties. In Co metal, the Fermi energy lies in the minority spin states, in a region where majority [$s(\uparrow)$] states are also found. Removal of these s states by ionization (forming Co^{2+} from Co) is an essential ingredient in rendering the system half metallic.

Panel (c) of this figure is the total DOS of non-magnetic semiconducting FeS_2 distributed equally between the two spin states. We have coincided s states of S (in the region -20 eV to -10 eV with respect to the Fermi energy, not shown) by shifting the origin on the energy axis for the DOS of FeS_2 , in order that the Fermi energy is fixed to the Fermi energy of CoS_2 . The assumption is that S s is a core state which should not be affected by compound formation. FeS_2 is a semiconductor with a calculated band gap of about 0.8 eV.³¹ In both FeS_2 and CoS_2 , p states of S below E_F extend from about -8 eV to -2.5 eV. In CoS_2 , Co d states (the t_{2g} manifold) start at -2.5 eV where S p states terminate. In

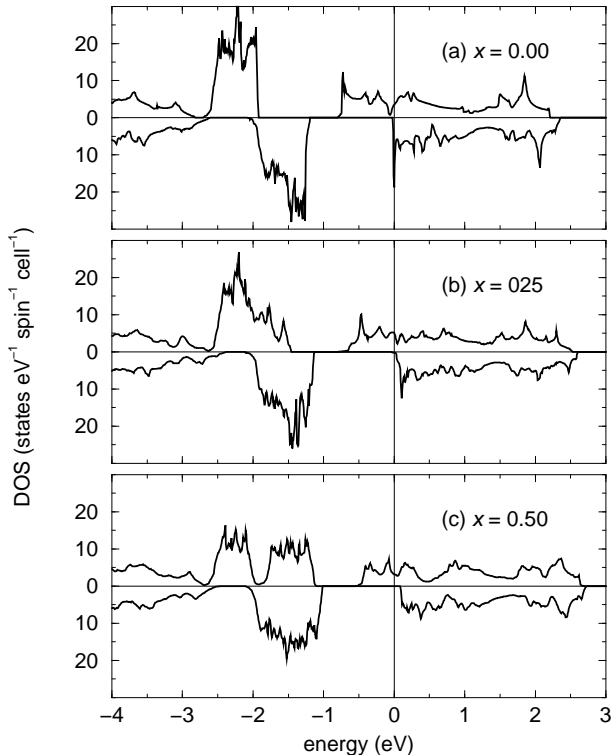


FIG. 6: Evolution of total LMTO densities of state as a function in x in $\text{Co}_{1-x}\text{Fe}_x\text{S}_2$: (a) CoS_2 ($x = 0.00$), (b) $\text{Co}_{0.75}\text{Fe}_{0.25}\text{S}_2$, ($x = 0.25$), and (c) $\text{Co}_{0.50}\text{Fe}_{0.50}\text{S}_2$, ($x = 0.50$).

FeS_2 , there is a gap between occupied S p states and the metal t_{2g} manifold. Comparing the DOS of FeS_2 with CoS_2 , we observe that the d manifold in the former is shifted to higher energies. This is indicative of the general trend amongst the first row transition metals that as one goes to the right (from Sc through Cu), metal d levels are stabilized. To some extent, this trend is reflected in the Pauling electronegativities which are 1.83 for Fe and 1.88 for Co. It is the same trend which shifts MX_2 crystal structures from being layered (with M^{4+}) to being three-dimensional (with M^{2+}) in a process referred to as redox competition.³² In oxide materials, the descent of cation d levels as one traverses first row transition metals results in the famous Zaanen-Sawatzky-Allen phase diagram.³³ In making solid solutions of CoS_2 and FeS_2 , we believe the distinctly shifted d levels of FeS_2 have a role to play. While substitution of Co by Fe in the series $\text{Co}_{1-x}\text{Fe}_x\text{S}_2$ results in electrons being removed from the e_g manifold, the d levels themselves are pushed to higher energies; the species (Fe) which “removes” electrons actually creates donor states. This is one of the factors which affects the electronic structure across the solid solution. A more electronegative substituent might remove electrons from p states of S, and this would be disastrous for the magnetism as demonstrated presently.

We have performed LMTO calculations on ordered supercells of pyrite CoS_2 after systematically replacing

some of the Co by Fe. Lattice a and internal structural parameters x_S for the calculations were taken from structure refinements of the nearest compositions as summarized in FIG. 2(b). In FIG. 6 shows densities of state for $\text{Co}_{1-x}\text{Fe}_x\text{S}_2$, for (a) $x = 0.00$, (b) $x = 0.25$, and (c) $x = 0.50$. In all three compounds, the shape of unfilled states just above E_F is “box-like” rising sharply with energy. The evolution of t_{2g} states with Fe substitution (in both spin directions) seems to result from a weighted superposition of the t_{2g} states of spin-polarized CoS_2 and non-magnetic FeS_2 [shown in FIG. 5(b and c)]. Filled t_{2g} levels below E_F seem pinned firmly in place. Partially filled e_g levels are shifted up in energy, to near (the respective) Fermi energies.³⁴ A feature of note is that at E_F , (the few) states in the minority states are progressively removed as x increases in $\text{Co}_{1-x}\text{Fe}_x\text{S}_2$. This result, as previously reported in the calculations of Mazin,⁶ explains the less-than-perfect [$(M/\mu_B)/\text{Co} < 1$] saturation magnetization of pure CoS_2 ($x = 0$), and the increased [$(M/\mu_B)/\text{Co} = 1$] magnetization as x increases, seen in our magnetic measurements, and in the measurements of Jarrett *et al.*⁴ From a magnetism viewpoint, the extent of half-metallicity in this system can be obtained as the ratio of the saturation magnetic moment in Bohr magnetons to the number of unpaired e_g electrons. Computationally, the magnetic moment, or more precisely, the polarization index P given by:³⁵

$$P = \left| \frac{N_{\uparrow}(E_F) - N_{\downarrow}(E_F)}{N_{\uparrow}(E_F) + N_{\downarrow}(E_F)} \right|$$

provides an indication of the half-metallicity. We calculate $P = 1$ for both the $x = 0.25$ and the $x = 0.5$ compounds. Correspondingly, magnetic moments *per* formula units were respectively obtained to be $0.748 \mu_B$ and $0.500 \mu_B$; whereas for CoS_2 ($x = 0$) it was $0.898 \mu_B$.

The COHP¹⁹ is a very useful tool for mapping the energy dependence of pairwise bonding and antibonding interactions between atoms from first-principles electronic structure calculations, including in systems which are spin-polarized.^{36,37} Figure 7(a) shows pairwise Co-S and S-S COHPs of parent *non-magnetic* CoS_2 , scaled by 0.5. We have verified that the spin-orbit coupling is negligible. Interactions are therefore confined to separate spin channels. Non-magnetic CoS_2 has sharply antibonding states at the E_F . Switching on spin-polarization decreases these antibonding states, in keeping with the suggestion of Landrum and Dronskowski³⁶ that sharply peaked antibonding COHPs in non-magnetic calculations can be an indicator (the equivalent of a Stoner criterion) of the electronic instability associated with spin polarization and ferromagnetism.

From FIG. 7(b), we observe bonding Co-S COHPs in the region of t_{2g} states and antibonding COHPs corresponding to the region of e_g states. E_F in spin-polarized CoS_2 falls in a gap flanked by antibonding Co-S(\uparrow) and antibonding Co-S(\downarrow). The S-S COHP in FIG. 7(c) shows the strongly bonding region where the p states of S are

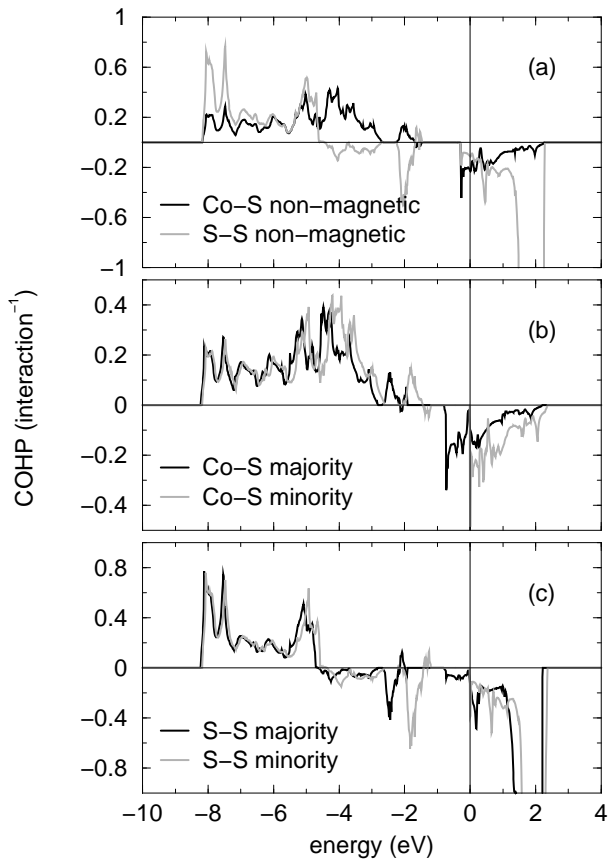


FIG. 7: (a) LMTO COHPs of non-magnetic CoS_2 showing Co-S and S-S interactions. The non-magnetic COHP has been scaled by a factor of 0.5. (b) LMTO COHPs of the Co-S interactions in CoS_2 in the two spin directions. (c) LMTO COHPs of the S-S interactions in CoS_2 in the two spin directions. In the definition we employ here, positive COHPs correspond to bonding interactions and negative COHPs to antibonding interactions. This is the opposite to the convention used in the original paper.¹⁹

found. The effect of spin-polarization on S-S COHPs is small but important. Interestingly, the antibonding region of the S-S(\uparrow) COHP just above E_F is slightly stabilized by spin-polarization, just as antibonding S-S(\downarrow) is slightly destabilized. Antibonding S-S(\uparrow) states are what pin the Fermi energy, and are perhaps the most significant states for discussing half-metallicity in these compounds. S-S states are pseudo-molecular so they do not disperse very greatly. They can be expected to remain in place because there is no great change in the charge state or in the degree of charge-transfer in the system as x is increased, as was observed from the constancy of the S-S distance. For antibonding S-S(\downarrow) states to descend through the Fermi energy, the S-S bond would have to be elongated.

In support of our argument that the S_2^{2-} units play a crucial role in determining the electronic structure of CoS_2 and the series $\text{Co}_{1-x}\text{Fe}_x\text{S}_2$, we have performed first-

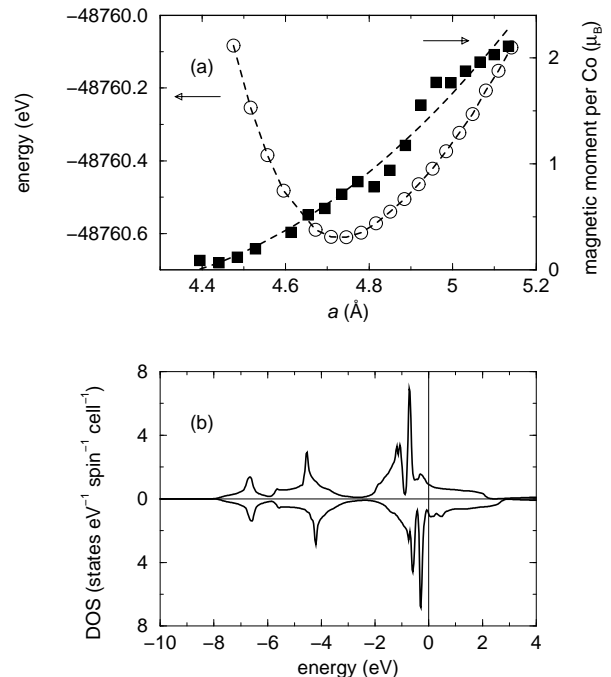


FIG. 8: (a) Total energy and magnetic moment *per Co atom* in rock-salt CoS as a function of the cubic cell parameter, as obtained from spin-polarized LAPW calculations. (b) Total Densities of state in the two spin directions of ferromagnetic CoS , calculated for a rock salt ($Fm\bar{3}m$) structure with $a = 4.67 \text{ \AA}$.

principles calculations on hypothetical rock-salt CoS , which has approximately the same atomic topology, and the same formal Co valence as pyrite CoS_2 . Figure 8(a) shows the results of the structure optimization by plotting total energy as a function of the cubic cell parameter, as well as the corresponding magnetic moment of Co. The GGA-optimized cell parameter was determined to be 4.67 \AA . The corresponding magnetic moment is about $0.5 \mu_B$ *per Co*. Figure 8(b) shows the densities of state of ferromagnetic CoS in the two spin directions. It is seen that the crystal field in CoS is much smaller than in CoS_2 . More importantly, CoS is not a magnetic half-metal, despite minority spin states trying to nest in a pseudogap. The electronic structure is characteristic of so-called “intermediate spin” systems such as the finite-temperature electronic structure of the cobalt oxide perovskite LaCoO_3 .³⁹

V. CONCLUSIONS

The low Curie temperatures of $\text{Co}_{1-x}\text{Fe}_x\text{S}_2$ make their use as spin injectors in spintronic circuitry unlikely.³⁸ This system does however offer insights into the design of new half-metallic magnets. There are two questions which our results help to address. The first is, what renders a compound half-metallic? From observing changes

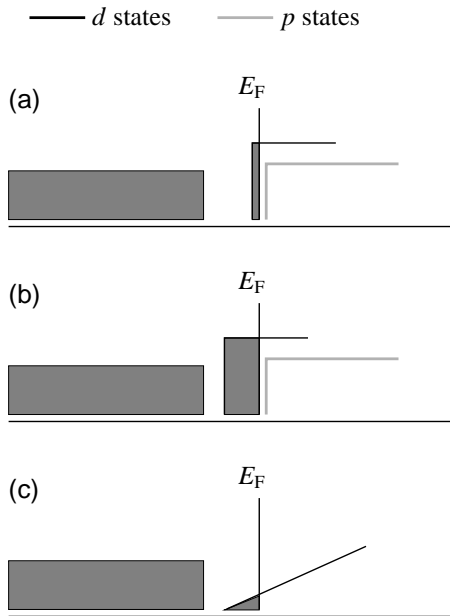


FIG. 9: (a) Summary of the non-magnetic electronic structure of $\text{Co}_{1-x}\text{Fe}_x\text{S}_2$ for large x values (low e_g filling). As x becomes slightly less than 1, the e_g levels are filled and descend below E_F . The p states remain above E_F however. The box-like shape of the unfilled d states ensures the Stoner criterion is satisfied even for small filling. (b) Even at larger e_g filling (smaller x), only d states descend below E_F , and E_F is pinned to the bottom of the unfilled p states. (c) Schematic non-magnetic states in a more usual material such as CoS , where unfilled states grow gradually, and the Stoner criterion is satisfied only for large filling.

on going from ferromagnetic Co metal to CoS_2 , we learn that s and p states at E_F (present in Co) are not good for half-metallic behavior since they are only poorly exchange split. Compound formation through removal of

s and p electrons is therefore useful. This suggests that even in systems such as the Heusler compounds, X_2YZ , where X and Y are usually transition elements and Z is a main group element, it might help to have electronegative substituents at Z (for example, Si rather than Al).⁴⁰

The second question is how the system retains ferromagnetism and half-metallicity across the substitution range. We summarize our findings on the unusual electronic structure of the pyrites solid solutions $\text{Co}_{1-x}\text{Fe}_x\text{S}_2$ in the scheme displayed in FIG. 9. For low filling of e_g states (x approaching 1), the electronic structure is characterized by “box-like” states above E_F , with a very sharp rise in the number of states with energy, as depicted in FIG. 9(a and b). The origins of this sharp rise, as we have demonstrated, are S-S antibonding states, which persist just above the E_F through the solid solution series. The states are sharp because they are pseudo-molecular. Even small filling of empty states results in the Stoner criterion being fulfilled⁶ and the rapid onset of ferromagnetism.^{4,11} The important role played by the shape of the DOS in fulfilling the Stoner criterion has been examined in detailed for transition metals by Andersen *et al.*⁴¹

Acknowledgments

We thank J. Gopalakrishnan for pointing us towards CoS_2 and Ryan Hummel (IGERT undergraduate intern) for help with sample preparation. Discussions with, and help from Ole Andersen, Nicola Spaldin, Kiril Katsov, and Pio Baettig are gratefully acknowledged. This work was partially supported by the MRL program of the National Science Foundation under the Award No. DMR00-80034, including a seed grant. CE thanks Nicola Spaldin and the Materials Research Laboratory for support.

* Electronic address: ramesha@engineering.ucsb.edu

† Electronic address: seshadri@mrl.ucsb.edu

‡ Electronic address: ederer@mrl.ucsb.edu

§ Electronic address: tao.he@usa.dupont.com

¶ Electronic address: mas.subramanian@usa.dupont.com

¹ S. Das Sarma, *Am. Sci.*, **89**, 516 (2001); D.D. Awschalom, M.E. Flatté, and N. Samarth, *Sci. Am. (Int. Ed.)* **286**, 66 (2002); N.A. Spaldin, *Magnetic Materials, Fundamentals and Device Applications* (Cambridge University Press, Cambridge, England, 2003).

² J.M.D. Coey and S. Sanvito, *J. Phys. D. Appl. Phys.* **37**, 988, (2004).

³ J.E. Pask, L.H. Wang, C.Y. Fong, W.E. Pickett, and S. Dag, *Phys. Rev. B.* **67**, 224420 (2003).

⁴ H.S. Jarrett, W.H. Cloud, R.J. Bouchard, S.R. Butler, C.G. Frederick, and J.L. Gillson, *Phys. Rev. Lett.* **21**, 617 (1968).

⁵ G.L. Zhao, J. Callaway, and M. Hayashibara, *Phys. Rev.*

B. **48**, 15781 (1993).

⁶ I.I. Mazin, *Appl. Phys. Lett.* **77**, 3000 (2000).

⁷ L. Wang, T.Y. Chen, and C. Leighton, *Phys. Rev. B.* **69**, 094412 (2004).

⁸ C.N.R. Rao and K.P.R. Pisharody, *Prog. Solid State Chem.* **10**, 207, (1976).

⁹ F. Hulliger and E. Mooser, *J. Phys. Chem. Solids* **26**, 429 (1965).

¹⁰ L. Néel and R. Bénéot, *C. R. Acad. Sci.* **237**, 444 (1953).

¹¹ J.F. DiTusa, S. Guo, D.P. Young, R.T. Macaluso, D.A. Browne, N.L. Henderson, and J.Y. Chan, *cond-mat/0306541*.

¹² R.A. de Groot, F.M. Mueller, P.G. van Engen, and K.H.J. Buschow, *Phys. Rev. Lett.* **50**, 2024 (1983).

¹³ H. Yamada, K. Terao, and M. Aoki, *J. Magn. Magn. Mater.* **177-181**, 607 (1998).

¹⁴ S.K. Kwon, S.J. Youn, and B.I. Lim, *Phys. Rev. B.* **62**, 357 (2000).

- ¹⁵ T. Shishidou, A.J. Freeman, and R. Asashi, *Phys. Rev. B* **64**, 180401 (2001).
- ¹⁶ S.F. Cheng, G.T. Woods, K. Bussmann, I.I. Mazin, R.J. Soulen, Jr., E.E. Carpenter, B.N. Das, and P. Lubitz, *J. Appl. Phys.* **93**, 6847 (2003).
- ¹⁷ H.M. Rietveld, *J. Appl. Cryst.* **2**, 65 (1969).
- ¹⁸ O. Jepsen and O.K. Andersen, The STUTTGART TB-LMTO-ASA Program version 47, MPI für Festkörperforschung, Stuttgart, Germany, 2000.
- ¹⁹ R. Dronskowski and P.E. Blöchl, *J. Phys. Chem.* **97**, 8617 (1993).
- ²⁰ J.-F. Bézar and P. Garnier, Computer code XND, 1992, available from the website at <http://www.ccp14.ac.uk>
- ²¹ O.K. Andersen, *Phys. Rev. B* **12**, 3060 (1975).
- ²² J.P. Perdew and Y. Wang, *Phys. Rev. B* **33**, 8800 (1986); J.P. Perdew, J.A. Chevary, S.H. Vosko, K.A. Jackson, M.R. Pederson, D.J. Singh, and C. Fiolhais, *C. Phys. Rev. B* **46**, 6671 (1992).
- ²³ U. von Barth and L. Hedin, *J. Phys. C* **5**, 1629 (1972).
- ²⁴ C. Ederer, M. Komelj, M. Fähnle, and G. Schütz, *Phys. Rev. B* **66**, 094413 (2002)
- ²⁵ A.H. MacDonald, W.E. Pickett, and D.D. Koelling, *J. Phys. C: Solid State Phys.*, **13**, 2675 (1980).
- ²⁶ G.K.H. Madsen, P. Blaha, K. Schwarz, E. Sjöstedt, and L. Nördström, *Phys. Rev. B* **64**, 195134 (2001). See <http://www.wien2k.at>
- ²⁷ J.P. Perdew, K. Burke, and M. Ernzerhof, *Phys. Rev. Lett.* **77**, 3865 (1996).
- ²⁸ R.D. Shannon and C.T. Prewitt, *Acta Crystallogr., Sect. B: Struct. Crystallogr. Cryst. Chem.* **25**, 925 (1969); R.D. Shannon, *Acta Crystallogr., Sect. A: Cryst. Phys., Diffr., Theor. Gen. Crystallogr.* **32**, 751 (1976).
- ²⁹ E. Nowack, D. Schwarzenbach, and T. Hahn, *Acta Crystallogr., Sect. B: Struct. Sci.* **47**, 650 (1991).
- ³⁰ S. Finklea, L. Cathey, and E.L. Amma, *Acta Crystallogr., Sect. A: Cryst. Phys., Diffr., Theor. Gen. Crystallogr.* **32**, 529 (1976).
- ³¹ V. Eyert, K.-H. Höck, S. Fiechter, and H. Tributsch, *Phys. Rev. B* **57**, 6350 (1998).
- ³² S. Jobic, R. Brec, and J. Rouxel, *J. Alloys Compounds* **178**, 253 (1992).
- ³³ J. Zaanen, G.A. Sawatzky, and J.W. Allen, *Phys. Rev. Lett.* **55**, 418 (1985).
- ³⁴ We find, using *s* states of S as a reference, that the calculated position of the Fermi energy shifts only very little across the solid solution series.
- ³⁵ J.M.D. Coey and M. Venkatesan, *J. Appl. Phys.* **91**, 6671 (8345).
- ³⁶ G.A. Landrum and R. Dronskowski, *Angew. Chem. Intl. Edn. Engl.* **38**, 1390 (1999); G.A. Landrum and R. Dronskowski, *Angew. Chem. Intl. Edn. Engl.* **39**, 1560 (2000).
- ³⁷ C. Felser and R. Seshadri, *Intl. J. Inorg. Mater.* **2**, 67 (2000).
- ³⁸ C. Palmström, *MRS Bulletin*, 725, October 2003.
- ³⁹ M. Imada, A. Fujimori, and Y. Tokura, *Rev. Mod. Phys.* **70**, 1235, (1998)
- ⁴⁰ I. Galanakis, P.H. Dederichs, and N. Papanikolaou, *Phys. Rev. B* **66**, (2002) 174429.
- ⁴¹ O.K. Andersen, J. Madsen, U.K. Poulsen, O. Jepsen, and J. Kollár, *Physica B*, **86-88**, 249 (1977).